Nonlinear Viscoelastic Properties of Layered-Silicate-Based Intercalated Nanocomposites

Jiaxiang Ren and Ramanan Krishnamoorti*

Department of Chemical Engineering, University of Houston, Houston, Texas 77204-4004

Received March 18, 2002

ABSTRACT: The nonlinear viscoelastic properties for a series of intercalated nanocomposites of an organically modified montmorillonite and a disordered styrene−isoprene diblock copolymer are reported. The linear-to-nonlinear transition for stress relaxation measurements, the applicability of time−strain separability, and the associated damping function are examined. The nanocomposites exhibit strong shear-thinning behavior thought to result from orientation of the layers in response to the applied shear deformation. We demonstrate that the empirical Cox−Merz rule is inapplicable for such nanocomposites and that steady and dynamic oscillatory flow are not equivalent for such mesostructured materials. The K-BKZ constitutive model is used to predict the steady shear properties from the experimentally measured linear stress relaxation and stress relaxation based damping behavior. While being able to reasonably capture the low shear rate shear stress properties, this empirical model breaks down in trying to model the shear stress behavior at intermediate shear rates and the normal stress behavior at all shear rates and silicate loadings.

Introduction

Recently, much interest has focused on the development of polymer nanocomposites prepared by dispersing inorganic nanoparticles in a polymer matrix and achieving a combination of mechanical, physical, and thermal properties at extremely low loadings of the inorganic species.[1−3] Among such nanocomposites, hybrids prepared with layered silicates have attracted significant attention because of the relative ease of obtaining the minerals,[4,5] the early commercialization of products,[6] and the ability of these systems to provide model systems to examine the structure and dynamics of confined and near-surface polymers.[2,7−10]

Melt state viscoelastic properties of such layered silicate-based nanocomposites have attracted significant attention because of their sensitivity to the mesoscale structure and their importance in understanding the processability of such hybrid materials.[7,8,11−18] It has been suggested that the formation of a superstructure of the dispersed layers in the polymer matrix dominates the linear viscoelastic properties of these nanocomposites.[7,8,11,12] Some of the resultant rheological characteristics are similar to those observed in colloidal dispersions, emulsions, pastes, and liquid crystals and unified under materials termed as soft glassy materials.[19] These materials exhibit rheological properties resulting from their intrinsically metastable and disordered structure similar to that observed in polymer layered-silicate nanocomposites.[19,20]

In previous papers, we have reported the melt-state linear viscoelastic properties of polymer layered-silicate nanocomposites. Studies were performed on nanocomposites prepared with poly(dimethylsiloxane),[2,17] end-tethered poly(ϵ-caprolactone), and nylon-6[2,8,15,18] and with ordered and disordered polystyrene−polyisoprene (PS−PI) block copolymers.[7,11−13,16] The layered silicates employed belonged to the general class of 2:1 smectites with effective disk diameters ranging from 30 nm to 10 μm and were organically modified to render hydrophobic.[5,9,11] For the case of a nearly symmetrical disordered PS−PI block copolymer (PSPI18) and a dimethyldioctadecylammonium-substituted montmorillonite (2C18M) nanocomposite, we found that, while the chain relaxation is independent of the silicate loading, the long time response was significantly altered, particularly at high silicate loadings (i.e., with 6.7 wt % or greater of layered silicate).[12,16] The observed quiescent-state solidlike linear dynamic oscillatory behavior and linear stress relaxation behavior observed for these high silicate nanocomposites are conjectured to result from the development of a three-dimensional percolated network mesostructure.[3,12] Further, this quiescent superstructure is highly susceptible to change upon application of shear, and in fact, in steady shear even at the lowest shear rates probed significant alignment of the layers is observed.[16] At higher shear rates the alignment is significantly enhanced and leads to steady-state viscosity and elasticity properties of these hybrids to start to resemble that of the unfilled polymer.[11,16]

In this paper we extend the previous study to the examination of nonlinear shear properties of the hybrids composed of the disordered polystyrene−polyisoprene diblock copolymer and the organically modified (2C18) montmorillonite. This will provide a more detailed understanding of the response of such anisotropic materials to the application of shear.[21] Further, as demonstrated by previous studies of block copolymer micelles,[22] such a study would provide complementary insight into the complex relaxation behavior of structured polymeric fluids. Finally, we attempt to examine the linear and nonlinear shear measurements in the context of a fairly powerful integral constitutive equation, the K-BKZ equation, and determine the regimes over which such a simple model is able to capture the rheological response quantitatively.

Experimental Methods

A disordered nearly symmetric diblock copolymer of styrene and 1,4-isoprene (PSPI18) ($M_w \sim 17\,700$, $M_w/M_n < 1.07$, $\phi_{PS} \sim$

* To whom correspondence should be addressed. E-mail: ramanan@uh.edu.

10.1021/ma020412n CCC: $25.00
Published on Web 05/20/2003

0.44, and T_{ODT} < 80 °C) and a dimethyldioctadecylammonium-substituted montmorillonite (2C18M) (~0.95 nm thick silicate layers with disk diameters of 0.2−0.5 μm) are the components of the nanocomposites, and their characterization has been described extensively in previous papers.[7,12,16,23] Nanocomposites were prepared by mixing appropriate quantities of finely ground 2C18M with PSPI18 in toluene at room temperature followed by extensive drying and subsequent annealing in a vacuum oven at 100 °C for 10 h. Four hybrids with silicate concentration of 2.1, 3.5, 6.7, and 9.5 wt % were prepared for the study. X-ray diffraction reveals the development of intercalated nanocomposites with a gallery height of ~2.5 nm, ~0.4 nm larger than that for polystyrene + 2C18M nanocomposites.

Melt-state rheological measurements were performed on a Rheometric Scientific ARES rheometer equipped with a transducer capable of measuring torques over the range of 0.2−2000g_f cm and normal forces over the range of 2−2000g. A cone-and-plate fixture with a plate diameter of 25 mm and a cone angle of 0.1 rad was used in this work. In stress relaxation measurements, a single step strain with amplitude γ was applied at time $t = 0$, and the resulting shear stress $\sigma_{12}(t,\gamma)$ was monitored as a function of time. The modulus $G(t,\gamma)$ was determined as

$$G(t,\gamma) = \frac{\sigma_{12}(t,\gamma)}{\gamma} \tag{1}$$

Quiescent periods of 500−10 000 s between succeeding measurements were implemented to allow the samples to equilibrate, with the longer quiescent periods typically implemented for the larger strain amplitudes and nanocomposites with higher silicate fraction. Data at small step strains were reproducible after application of large step strains, provided a sufficient rest time was allowed between rheological tests. In fact, this reproducibility was used as a metric to determine the length of the quiescent period. A similar protocol of rest or quiescent periods following testing and verification of the reproducibility of data at low shear rates was also implemented for the steady shear start-up measurements. Start-up measurements were implemented for each sample over a range of shear rates ($0.01 \le \dot{\gamma} \le 100$ s^{-1}) and performed until all viscoelastic functions achieved steady values at each shear rate. The steady-state shear stress σ_{12} (and thus the viscosity) and first normal stress difference N_{12} (= $\sigma_{11} - \sigma_{22}$) were monitored and reported here.

On the other hand, the nonlinear oscillatory flow properties were studied by the successive application of sinusoidal strain signals at a constant frequency ω of the form $\gamma(t) = \gamma_0 \sin(\omega t)$, where γ_0 is the strain amplitude and allowed to vary from 0.01 to 300%. Measurements were performed successively over logarithmically spaced strain amplitudes with no rest or quiescent periods between data points. The data were interpreted in terms of the linear viscoelastic functions by analyzing the measured shear stress $\sigma(t) = \gamma_0 (G' \sin(\omega t) + G'' \cos(\omega t))$, where G' and G'' are the storage and loss modulus, respectively. In addition, we report the data in terms of the dynamic viscosity, i.e., $\eta^*(\omega) = G^*(\omega)/\omega = [(G')^2 + (G'')^2]^{1/2}/\omega$, and use this function to compare the oscillatory flow behavior to the steady shear viscosity $\eta(\dot{\gamma})$.

Results and Discussion

Stress Relaxation Behavior. We first discuss the strain amplitude dependence of the stress relaxation behavior of the polymer and the nanocomposites. The linear stress relaxation behavior (in quantitative agreement with linear dynamic oscillatory properties) demonstrated a gradual change from liquid to solidlike behavior with increasing layered silicate content.[12] We had previously attributed this to the presence of a hydrodynamically percolated layered silicate layers or tactoids resulting in solidlike behavior.[7,11,12,16] Here we examine the influence of larger strain amplitudes on

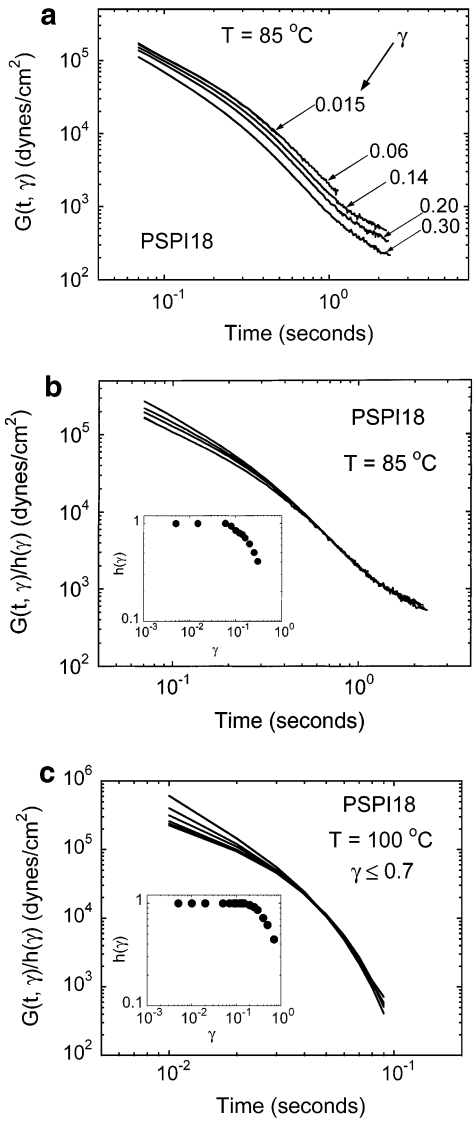

Figure 1. (a) Strain amplitude dependence of the stress relaxation behavior of PSPI18 at 85 °C. The data for $\gamma < 0.06$ merge onto a single line and correspond to the linear stress relaxation behavior. (b) Time−strain superposed stress relaxation master curves for PSPI18 at 85 °C obtained by vertical shifting of $G(t,\gamma)$ (shown in a) by a factor of $1/h(\gamma)$ (shown in the inset) to achieve the best superposition on the $G(t)$ curve for $t \ge 0.3$ s. The data beyond γ of 0.3 did not merge onto this master curve and demonstrate the failure of time−strain separability for modest strain amplitudes. (c) Similar time−strain superposed master curve for PSPI at 100 °C. The linear regime and the strains over which time−strain superposability is applicable is considerably extended to that observed at 85 °C.

that quiescent superstructure by examining the changes in the stress relaxation behavior.

The amplitude dependence of the single step-strain stress relaxation behavior for the unfilled polymer at T = 85 °C is shown in Figure 1a. The data are independent of strain amplitude for $\gamma \le 0.06$ and exhibit shear thinning behavior for $\gamma > 0.06$. The data ($G(t,\gamma)$) displayed in Figure 1a (i.e., for $\gamma \le 0.3$) are consistent with that of a narrow molecular weight distribution polymer[24] and obey the principle of time−strain factorability:

$$G(t,\gamma) = G(t)\, h(\gamma) \quad \text{for } t \ge \tau \tag{2}$$

where $G(t)$ is the linear stress relaxation behavior, $h(\gamma)$

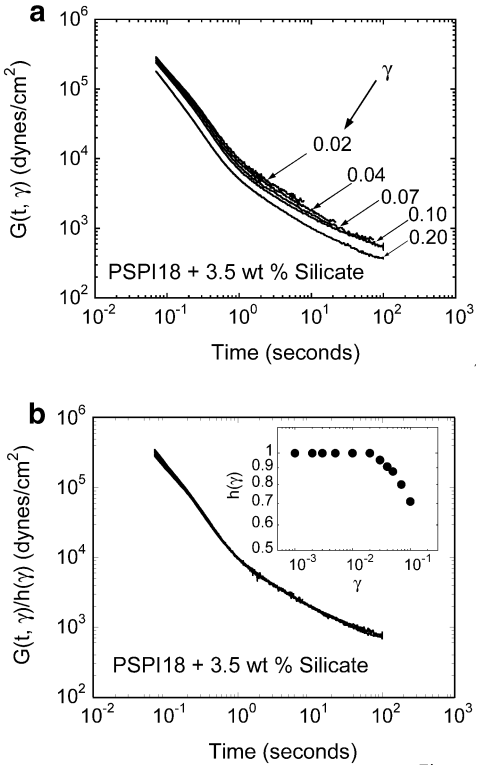

Figure 2. (a) Strain dependence of the stress relaxation behavior for PSPI18 + 3.5 wt % 2C18M at 85 °C. The stress relaxation behavior is linear up to the strain amplitude 0.02. (b) Time−strain superposed stress relaxation master curves obtained by vertical shifting of data shown in (a) by a factor of $1/h(\gamma)$ to achieve the best superposition on the $G(t)$ curve for $t \geq 0.3$ s. The data beyond γ of 0.1 did not merge onto this master curve.

is the damping function, and τ is the relaxation time of the polymer. At short times (i.e., $t < 0.4$ s; $\tau \sim 1.2$ s at 85 °C) there is failure of time−strain superpositioning, and this behavior is consistent with previous observations for homopolymers and homopolymer solutions.[25] Master curves for the unfilled polymer were only generated up to modest strain amplitudes; beyond $\gamma \sim 0.3$, the shape of the stress relaxation was altered and could not be superposed. We attribute this failure of time−strain superposability at high strain amplitudes and the early onset of shear thinning to the proximity of the measurement temperature to the order−disorder transition temperature (T_{ODT}) of the block copolymer and the possible coupling of the concentration fluctuation and the applied shear.[26,27] On the basis of the molecular weight, composition of the copolymer, and the thermodynamic interactions between PS and PI,[27,28] we anticipate that PSPI18 has a T_{ODT} slightly lower than 80 °C. On the other hand, at a measuring temperature of 100 °C the onset of shear thinning was considerably delayed, and time−strain separability was applicable over a much larger strain window as demonstrated in Figure 1c. Han and Kim have observed similar failure of time−strain separability for a thermotropic liquid crystalline polymer in the nematic state.[29] However, for the same polymer, in the isotropic state, time−strain factorability was observed.

The strain dependence of the stress relaxation behavior and the applicability of time−strain separability for a typical nanocomposite are shown in Figure 2. The nanocomposites exhibit similar shear-thinning behavior with a lower onset strain amplitude (Figure 3). Further,

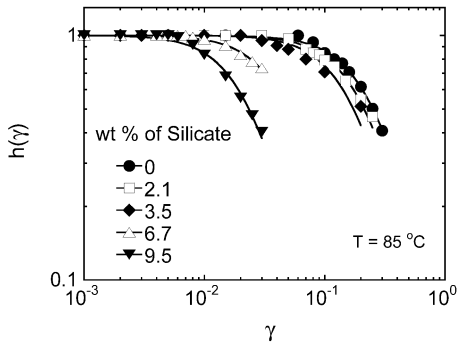

Figure 3. Silicate content dependence of the damping functions $h(\gamma)$ for PSPI18 and PSPI18 + 2C18M nanocomposites at 85 °C. The solid curves represent the empirical fitting to eq 5, with the parameters tabulated in Table 1. It is evident that the onset of strain softening occurs at lower strain amplitudes with increasing silicate content.

Table 1. Fitting of $h(\gamma)$ to Eq 3

hybrid composition (wt % silicate)	α
0	15.7 ± 0.6
2.1	22.1 ± 0.9
3.5	33.2 ± 3.8
6.7	429 ± 17
9.5	1817 ± 94

the strain dependence of $h(\gamma)$ is adequately fitted, as shown in Figure 3, by an empirical relationship frequently used to model the damping behavior in complex microstructured systems:[24,30]

$$h(\gamma) = \frac{1}{1 + \alpha\gamma^2} \tag{3}$$

with the values of α tabulated in Table 1. α increases with increasing silicate loading: changing slowly for nanocomposites with 0, 2.1, and 3.5 wt % silicate and then changing dramatically for the hybrids with 6.7 and 9.5 wt % silicate. The onset strain for shear thinning decreases with increasing silicate loading and exhibits a substantial drop between the 3.5 and 6.7 wt % hybrids. Additionally, for those two nanocomposites the principle of time−strain separability appears to be valid over a much smaller strain window as compared to the polymer, with the modulus data at high strains demonstrating a different shape compared to those at low strains. We note that previously Macklay and co-workers have tested a Wagner type damping function ($h(\gamma) = \exp(-k\gamma^n)$) for various polymeric and colloidal fluids.[31] While they found this model to work adequately for most of the classes of materials studies, for the case of kaolinite suspensions, most closely resembling the systems studied here, this Wagner type damping function was inappropriate.

We conjecture that, analogous to discotic liquid crystals and other mesostructured materials,[31−33] the highly anisotropic silicate layers or collections of silicate layers (i.e., tactoids) respond to the external flow and orient when subjected to moderate and large strain amplitudes. This results in the enhanced shear thinning for the nanocomposites as compared to the unfilled polymer. On the basis of the low volume fractions of added filler and the reproducibility of the shear thinning, alternate hypothesis such as confinement-induced shear thinning[34] or shear-induced disaggregation of the tactoids can be neglected.[11,16] Further, interactions between silicate layers (or between tactoids) are significant when

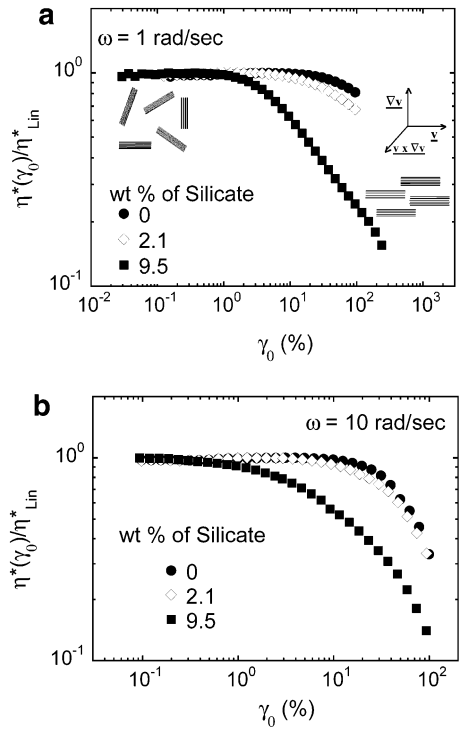

Figure 4. Strain amplitude dependence of the normalized complex viscosity (T = 85 °C), $\eta^*(\gamma_0)/\eta^*_{Lin}$, obtained in oscillatory mode for the unfilled PSPI18, 2.1, and 9.5 wt % silicate nanocomposites at ω = 1 rad/s (a) and at ω = 10 rad/s (b). The data at successive strain values were obtained with no quiescent period between data points. The onset of shear thinning depends strongly on the silicate content and in a weaker manner on the frequency of oscillation. The schematic orientation states for the nanocomposites at low strain amplitudes and high strain amplitudes are shown in (a) and are based on neutron and X-ray scattering studies.[8,15]

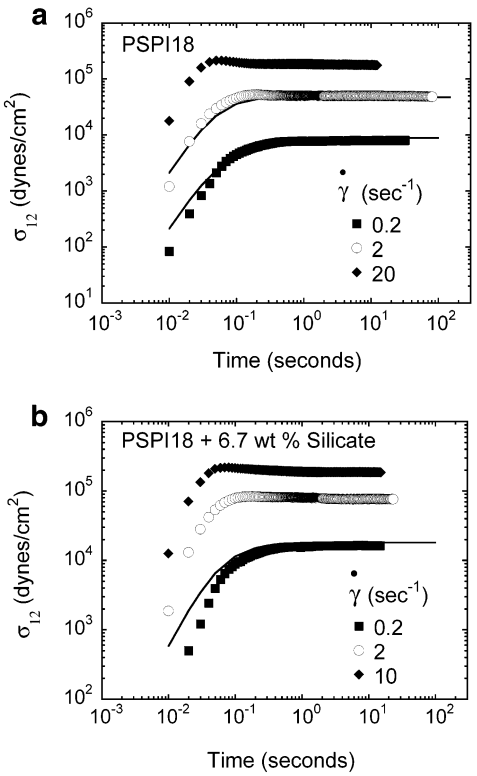

Figure 5. Transient development of the shear stress for the unfilled PSPI18 (a) and PSPI18 + 6.7 wt % 2C18M (b) following start-up from rest at three different shear rates at 85 °C. For purposes of comparison, the predictions of the K-BKZ equation (eq 9) are also shown. For the unfilled polymer and the nanocomposite, reasonable agreement of the experimental results and the predictions of the K-BKZ equation are realized at low shear rates.

the silicate loading is above the percolation value, and disruption of this mesostructure results in the enhanced damping behavior (and significantly increased value of α) for the 6.7 and 9.5 wt % silicate nanocomposites. The change in the quiescent mesostructure by relatively modest strains is surmised to result in the premature failure of the time−strain superposability for the higher silicate content nanocomposites.

Nonlinear Oscillatory Shear. To contrast and compare the influence of oscillatory strain to step strain, the strain amplitude dependence of the dynamic oscillatory viscoelastic properties of the nanocomposites was examined. The strain amplitude dependence of η^* (normalized by the linear values) at ω = 1 and 10 rad/s and T = 85 °C for three samples are reported in parts a and b of Figure 4, respectively. We justify the interpretation of the large-amplitude oscillatory data in terms of the linear parameters (G', G'', and η^*) because of the previously observed small higher (third and fifth) order harmonics, compared to the primary harmonic, of the oscillatory shear stress signal.[15,35] The data in Figure 4, like the stress relaxation data, indicate the lowering of the strain amplitude for onset of shear thinning with increasing silicate loading and suggest that the breakdown of the superstructure is responsible for the enhanced shear-thinning character of the nanocomposites. There is a mild dependence of this shear thinning on the measurement frequency, with the onset delayed to higher strain amplitudes for the lower frequency, and is consistent with the behavior of a material with a finite yield stress.[36]

In fact, similar to many other layered materials,[11,33,37] the prolonged application of large-amplitude oscillatory shear at a fixed frequency on these intercalated nanocomposites results in the "parallel" orientation of the silicate layers and manifested rheologically as a significantly reduced postalignment linear (small amplitude) G' and G'' in the terminal zone.[8,12,15] Further, a significant increase of the terminal zone frequency dependence of G' and G'' was observed and interpreted as being caused by the breakdown of the three-dimensional percolated nanoparticle structure. Thus, much like the stress relaxation behavior, the nonlinear oscillatory flow behavior is also dominated by the ability of the silicate layers to orient in response to the applied flow and the onset of orientation (as manifested rheologically) appears not to be directly related only to a critical displacement.[15] In this aspect these intercalated melt-mixed nanocomposites are significantly different from end-tethered exfoliated nanocomposites where a reversible strain hardening is observed and attributed to the stretching of the distorted chains in response to the shear.[15]

Steady Shear Measurements. The time-dependent shear stress data for the start-up of steady shear at different shear rates for the unfilled polymer and an intercalated nanocomposite with 6.7 wt % 2C18M are shown in Figure 5. Both exhibit viscoelastic behavior with the presence of a small stress overshoot at high shear rates and the achievement of steady state at shorter times for the higher shear rates. Further, the shear stress data do not exhibit any time-dependent oscillations as would be expected from anisotropic

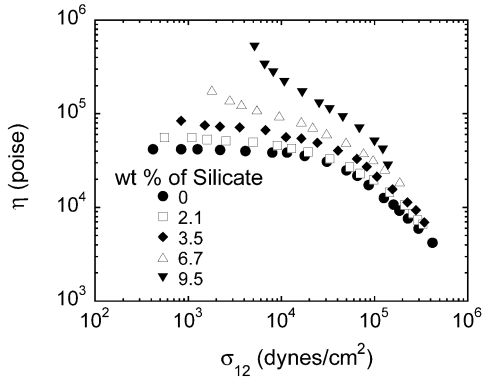

Figure 6. Dependence of $\eta(\dot{\gamma})$ on the shear stress σ_{12} at steady state for the nanocomposites with different silicate loading. Data were obtained from transient measurements described in Figure 5 and were obtained after prolonged periods of quiescent rest to allow the samples to lose any orientation imparted to them by the application of steady shear. The hybrids with silicate loading above 6.7 wt % display divergence of the viscosity and are consistent with the behavior of materials with finite yield stresses.

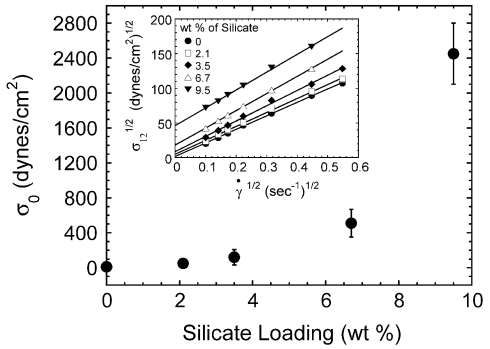

Figure 7. Concentration dependence of the yield stress σ_0, determined by the application of Casson's equation (eq 4) to the low shear rate steady shear data (as shown in the inset), for the nanocomposites. Within the error of the experiments, the yield stress is zero for PSPI18, and the hybrids with silicate loading below 3.5 wt %. The hybrids display significant yield stress when the silicate loading is above 6.7 wt %, and these are consistent with the inferences drawn from the linear oscillatory and stress relaxation behaviors regarding the existence of a filler network superstructure in these materials.

systems with particle tumbling or rotation.[38] The steady-state viscosity (η) as a function of the steady-state shear stress (σ_0) is shown in Figure 6. For the two hybrids with 6.7 and 9.5 wt % silicate, the data for η diverge and consistent with those exhibited by materials with a finite yield stress.[36,39] The yield stress is determined by fitting the low $\dot{\gamma}$ data to Casson's equation, given as[36,40]

$$\sigma_{12}^{1/2} = \sigma_0^{1/2} + \beta\,\dot{\gamma}^{1/2} \tag{4}$$

where σ_0 is the yield stress and β is an arbitrary constant. The fit to eq 4 and the yield stress determined are shown in Figure 7 and exhibit finite nonzero values for the nanocomposites with 6.7 and 9.5 wt % silicate. It is for these nanocomposites that we have previously hypothesized a quiescent-state percolated superstructure based on the solidlike dynamic oscillatory and linear stress relaxation moduli, diverging viscosities at low shear rates, and dramatically enhanced shear thinning observed in the damping function.

The divergence at low shear stresses (and low shear rates) observed in Figure 6 is also observed in many

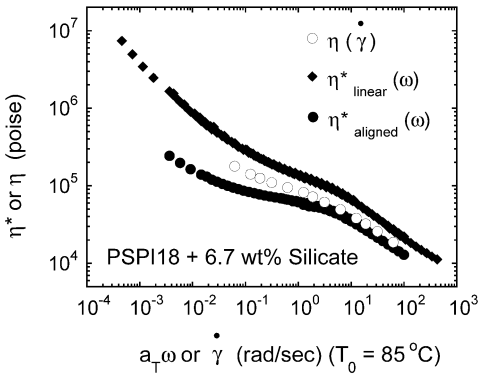

Figure 8. Test of the empirical Cox−Merz rule for the nanocomposite of PSPI with 6.7 wt % 2C18M. Master curves of the dynamic complex viscosity obtained from linear dynamic oscillatory measurement of the "as-loaded" randomly oriented nanocomposite (η^*_{linear}) are compared to the steady shear viscosity $\eta(\dot{\gamma})$, with η^*_{linear} exceeding $\eta(\dot{\gamma})$ for comparable shear rates. On the other hand, the linear dynamic complex viscosity after prolonged large-amplitude shear-induced alignment (η^*_{aligned}) is consistently lower than the $\eta(\dot{\gamma})$ at comparable shear rates. We thus conclude that steady shear, even at the lowest shear rates examined, leads to some alignment of the anisotropic silicate layers, resulting in the failure of the Cox−Merz rule for the nanocomposites.

other filled systems and thought to result from the formation of a filler network superstructure. In those cases the divergence occurs at much higher filler concentration: for example, for carbon black filled elastomer (isobutylene) comoposites (12 vol %)[3] and for glass fiber filled polypropylene composites (30 wt %).[41]

On the other hand, at high shear stresses (and high shear rates) the viscosity observed is comparable for the unfilled polymer and the nanocomposites. This behavior is thought to arise from the ability of the highly anisotropic layers (or tactoids) to be oriented by the applied flow and is similar to the response of many microstructured materials, particularly those possessing lamellar phases.[33] We note in passing that the transition to this high-shear rate behavior occurs at roughly the same shear rate for all the nanocomposites and is consistent with the previously suggested unchanged relaxation time for the polymer in the nanocomposites.

This ability to alter the mesoscale structure and orient the highly anisotropic silicate layers or tactoids of silicate layers results in the failure of the empirical Cox−Merz rule as demonstrated in Figure 8 for a 6.7 wt % 2C18M-based intercalated nanocomposite. The Cox−Merz rule requires that

$$\eta^*(\omega) = \eta(\dot{\gamma}) \quad \text{for } \omega = \dot{\gamma} \tag{5}$$

and is generally found to be applicable for homopolymers. In fact, for the unfilled disordered liquidlike block copolymer, the empirical Cox−Merz rule is applicable. On the other hand, for the nanocomposites examined, $\eta^*(\omega)$ always exceeds $\eta(\dot{\gamma})$, with the magnitude of the difference (at any shear rate) increasing with increasing silicate loading.

Such a failure of the Cox−Merz rule has been observed for other filled polymer systems and mesostructured materials[33] and suggests that the application of steady shear results in some preferential orientation of the initial quiescent random arrangement of the silicate layers or their tactoids. However, the dynamic viscosity after prolonged large-amplitude oscillatory shear alignment, $\eta^*_{\text{aligned}}(\omega)$, is less than $\eta(\dot{\gamma})$ at all shear

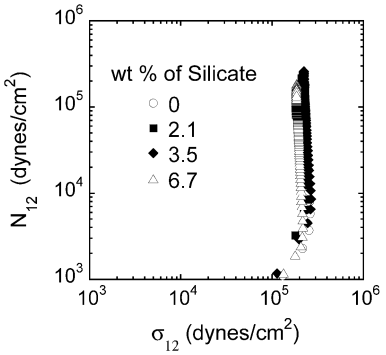

Figure 9. Dependence of N_{12} on σ_{12} for start-up measurements of the polymer and the nanocomposites where the steady-state values of N_{12} and σ_{12} roughly coincide for the different samples (start-up measurements for PSPI18: $\dot{\gamma} = 30$ s^{-1}, 2.1 wt %; 2C18M: $\dot{\gamma} = 20$ s^{-1}, 3.5 wt %; 2C18M: $\dot{\gamma} = 20$ s^{-1}, 6.7 wt %; 2C18M: $\dot{\gamma} = 10$ s^{-1}). The transient properties, while being similar, do not necessarily superpose.

rates, with the values becoming comparable at high shear rates. These data clearly demonstrate that low shear rate steady flow results in some orientation (considerably smaller than perfect "parallel" alignment) of the silicate layers and flows at high shear rates lead to substantial alignment of the silicate layers or tactoids of layers.

It has been reported previously that, unlike other filled systems, these layered-silicate-based nanocomposites demonstrate relatively small effects on the elasticity when compared at equivalent values of shear stress (see discussion below). The development of the transient N_{12} ($= \sigma_{11} - \sigma_{22}$) and σ_{12} from start-up exhibit only slight differences in the initial stages of the transient and the long-time (high σ_{12} and N_{12}) data being comparable (Figure 9). However, when compared at the same shear rate, the data for the unfilled polymer and the nanocomposites do not superpose (or appear self-similar) and do not result in the same final values of σ_{12} and N_{12}. These results suggest that the elasticity as measured by N_{12} is clearly a function of the shear stress σ_{12} generated and the ability to align the plates or disks results in similar enhancements in both σ_{12} and N_{12} for the nanocomposites as compared to the unfilled polymer.

Modeling of Data by a Constitutive Equation. We attempt to model the linear and nonlinear data using the K-BKZ integral constitutive equation model.[42] On the basis of the general elastic theory, which is independent of molecular structure, this constitutive equation has been shown to work well for the case of mesostructured block copolymer micelles and silica particle loaded polymer composites.[31] Following the Lodge model, the shear stress and first normal stress difference in simple shear are given as[43]

$$\sigma_{12}(t) = \int_{-\infty}^{t} m(t - t')\, h(\gamma)\, \gamma(t,t')\, \mathrm{d}t' \qquad (6)$$

$$N_{12}(t) = \int_{-\infty}^{t} m(t - t')\, h(\gamma)\, (\gamma(t,t'))^2\, \mathrm{d}t' \qquad (7)$$

where $m(t - t')$ is the linear viscoelastic memory function. For materials with known linear stress relaxation modulus and damping (nonlinear) behavior, the K-BKZ equation can be used to predict the shear stress and primary normal stress difference in other shear histories, such as double-step strain shear and steady shear. Here we use the K-BKZ equation to predict the start-up of steady flow and the shear rate dependence of the steady-state viscosity and the steady-state primary normal stress difference and compare them to the experimental data for the nanocomposites reported here. While the data for $h(\gamma)$ are provided in Figure 3 and adequately fitted by eq 3, a similar analytical expression is yet to be developed for the stress relaxation data, $G(t)$. Thus, prior to testing the predictions of the K-BKZ model, we develop an analytical description of the linear stress relaxation spectrum (presented in a previous paper[12]) by fitting to a sum of exponential decays as

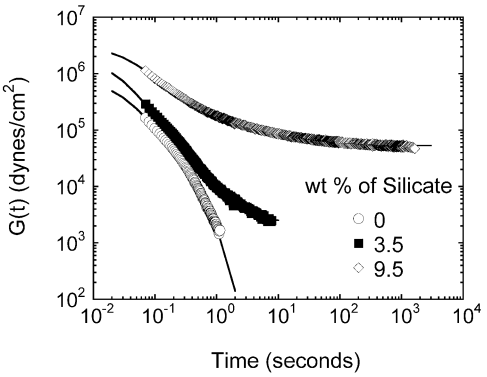

Figure 10. Time dependence of the linear stress relaxation modulus $G(t)$ at 85 °C for the unfilled PSPI18 and the hybrids with 3.5 and 9.5 wt % 2C18M nanocomposites. The solid lines represent the best fits of the data to the empirical eq 8 with the fitting parameters tabulated in Table 2.

Table 2. Fitting of Linear $G(t)$ to Eq 8

wt % silicate	i	G_i (dyn/cm^2) $\times 10^{-5}$	τ_i (s)
0	1	6.9 ± 0.2	0.027 ± 0.002
	2	1.63 ± 0.02	0.118 ± 0.002
	3	0.25 ± 0.01	0.386 ± 0.010
2.1	1	7.9 ± 0.5	0.031 ± 0.002
	2	1.95 ± 0.06	0.148 ± 0.003
	3	0.11 ± 0.01	1.27 ± 0.08
3.5	1	17. 4 ± 0.9	0.026 ± 0.002
	2	2.94 ± 0.06	0.090 ± 0.003
	3	0.85 ± 0.06	0.26 ± 0.01
	4	0.10± 0.01	1.64 ± 0.12
	5	0.025 ± 0.001	∞
6.7	1	20 ± 2	0.029 ± 0.002
	2	4.1 ± 0.3	0.13 ± 0.01
	3	0.82 ± 0.17	0.55 ± 0.11
	4	0.23 ± 0.03	5.1 ± 1.2
	5	0.086 ± 0.008	∞
9.5	1	36 ± 1	0.029 ± 0.002
	2	7.9 ± 0.1	0.147 ± 0.002
	3	1.84 ± 0.03	0.84 ± 0.02
	4	0.58 ± 0.01	8.3 ± 0.3
	5	0.19 ± 0.01	134 ± 6
	6	0.52 ± 0.02	∞

$$G(t) = \sum_{i=1}^{n} G_i \exp\left(-\frac{t}{\tau_i}\right) \qquad (8)$$

as shown in Figure 10. The fitted parameters G_i and τ_i for the unfilled polymer and the nanocomposites are tabulated in Table 2 and are used in the predictions of the K-BKZ equation. However, these are merely the best fits to the measured data, and aside from the near equivalence of the short relaxation processes, further interpretation of the relaxation spectrum in terms of physical parameters is not attempted.

For the start-up of shear flow, the shear stress growth function $\sigma_{12}(t,\dot{\gamma})$ and primary normal stress growth function $N_{12}(t,\dot{\gamma})$ can be described by

$$\sigma_{12}(t,\dot{\gamma}) = \int_0^t -\frac{dG(t')}{dt'} h(\gamma(t'))\,\gamma(t')\,dt' \quad (9)$$

$$N_{12}(t,\dot{\gamma}) = \int_0^t -\frac{dG(t')}{dt'} h(\gamma(t'))\,(\gamma(t'))^2\,dt' \quad (10)$$

where the cummulative strain, $\gamma(t')$ ($= \dot{\gamma} \otimes t$), is used to describe the displacement on the sample, and eqs 3 and 8 provide analytical descriptions of $h(\gamma)$ and $G(t)$, respectively. The transient start-up shear stress (σ_{12}) prediction is compared to the experimental data in Figure 5a,b for the unfilled polymer and a 6.7 wt % nanocomposite, with reasonable agreement observed at the lowest shear rates reported. However, at higher shear rates the experimental data and the predictions are not in quantitative agreement. On the other hand, at the highest shear rates the predictions were based on extrapolations of the stress relaxation function and thus considered unreliable and not shown here. We note that in all the comparisons we have only used ranges of strain where time−strain superposability was applicable and times accessed in the linear stress relaxation studies. Further, proof of the agreement at low shear rates for both the polymer and the nanocomposites is demonstrated in Figure 11, where the predictions of the steady shear viscosity are compared to the experimental data. Again at intermediate shear rates, the K-BKZ model underpredicts the experimental data.

On the other hand, in Figure 12a, we compare the predictions of the K-BKZ model to the experimental data for the shear rate dependence of the steady-state values of the primary normal stress difference (N_{12}). At all shear rates, we find that the model underpredicts the absolute value of N_{12}, although the shear rate dependences are similar. Further, discrepancies from the experimental data are demonstrated in Figure 12b, where the steady-state value of N_{12} is plotted against the steady state σ_{12}. While the experimental data demonstrate a silicate content independent "universal" behavior, the predictions show considerable silicate content dependent divergence. However, we note that while the experimental data are dominated by the high shear rate data, the K-BKZ model, as applied here, is unable to calculate the viscoelastic properties at high shear rates because of the necessity to extrapolate the linear stress relaxation modulus to shorter time scales than accessible experimentally and can only be used to predict the low shear rate dependence.

The K-BKZ model using linear stress relaxation modulus data and step-strain measurements to describe the nonlinear damping function is clearly inadequate to predict the intermediate shear rate viscosity data for the nanocomposites and the normal stress behavior at all shear rates. During the steady shear tests the sample slowly evolves to a final mesoscale oriented structure with the extent of orientation depending on the shear rate. The inability of the K-BKZ model to predict the intermediate shear rate data suggests that the nanocomposites undergo changes in their mesoscale structure at those shear rates that lead to rheological behavior not encountered in the determination of the damping functions via the step-strain measurements.

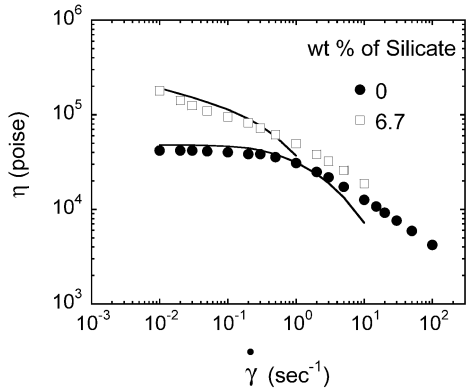

Figure 11. Comparison of the experimentally obtained and the theoretically predicted (using the K-BKZ equation) shear rate dependence of the steady-state viscosity $\eta(\dot{\gamma})$ for PSPI18 and the 6.7 wt % 2C18M nanocomposite. While reasonable agreement is observed at low shear rates, the K-BKZ prediction suggests a stronger shear-thinning character than observed experimentally.

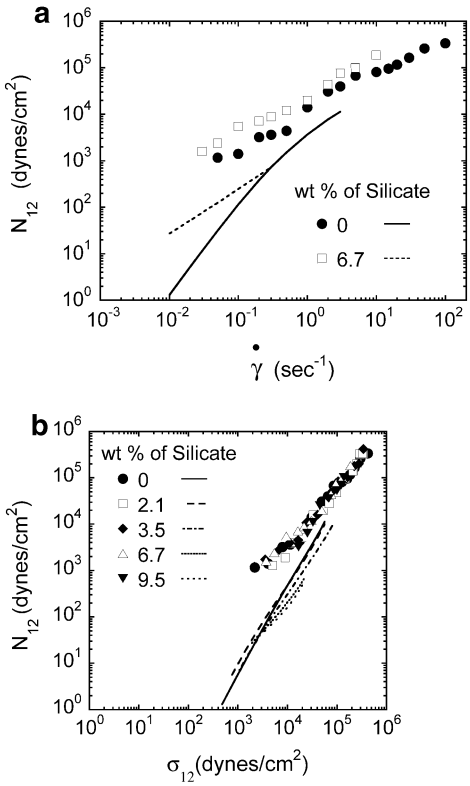

Figure 12. (a) Comparison of the predictions of the K-BKZ equation (lines) and the experimental data (symbols) for the shear rate dependence of the steady-state primary normal stress difference N_{12} for PSPI18 and the 6.7 wt % 2C18M-based nanocomposite. The K-BKZ equation underpredicts the experimental data at all shear rates. (b) Comparison of the experimentally obtained dependence of the steady-state N_{12} vs steady-state σ_{12} for all the samples, with the predictions of the K-BKZ predictions. While the experimental data are dominated by those obtained at high shear rates, the predictions of the K-BKZ model are restricted to low shear rates. Nevertheless, the K-BKZ model does not demonstrate the experimentally observed "universal" behavior and tends to underpredict the values of N_{12} consistently.

Concluding Remarks

The nonlinear properties of the layered-silicate-based polymer nanocomposites provide dramatic evidence of the anisotropic nature of the layered silicates (or silicate tactoids) dispersed in a polymer matrix. In addition to the early onset of shear-thinning character observed in the nonlinear stress relaxation behavior and the dynamic oscillatory experiments, these nanocomposites also demonstrate a failure of the Cox−Merz rule. Most

interestingly, we observe that prolonged application of large-amplitude oscillatory shear results in a dynamic viscosity that is lower than the steady shear viscosity at a comparable shear rate, whereas prior to such alignment the dynamic viscosity exceeded the steady shear viscosity. An empirical constitutive equation such as the K-BKZ equation along with experimentally determined linear stress relaxation and nonlinear damping behavior is able to capture the viscosity at low shear rates but is unable to predict the experimental data at intermediate shear rates; the model always predicts a more dramatic shear thinning than experimentally observed. We conjecture that under steady shear the mesoscale structure of the nanocomposites continues to evolve, and this evolution, particularly at intermediate and high shear rates, must lead to the failure of the K-BKZ model and suggest a substantial investigation directly of the structural changes during such flow processes. On the other hand, the K-BKZ model consistently fails to predict the normal stress behavior in the polymer and in the nanocomposites and suggests an inherent shortcoming of this model or its applicability to nanocomposite systems examined here.

Acknowledgment. We acknowledge financial support from the donors of the Petroleum Research Fund, administered by the American Chemical Society, from the Texas Coordinating Board (ATP), and from Exxon-Mobil Chemical Co., Baytown, TX. This work made use of TCSUH/MRSEC shared facilities supported by the state of Texas through TCSUH and by NSF (DMR-9632667). Useful discussions with Dr. Adriana Silva and Koray Yurekli are gratefully acknowledged.

References and Notes

(1) Vaia, R. A.; Giannelis, E. P. *MRS Bull.* **2001**, *26*, 394−401. Krishnamoorti, R., Vaia, R. A., Eds.; *Polymer Nanocomposites: Synthesis, Characterization, and Modeling*; American Chemical Society: Washington, DC, 2001; Vol. 804. Beecroft, L. L.; Ober, C. K. *Chem. Mater.* **1997**, *9*, 1302−1317. Ishida, H.; Campbell, S.; Blackwell, J. *Chem. Mater.* **2000**, *12*, 1260−1267.

(2) Giannelis, E. P.; Krishnamoorti, R.; Manias, E. P. *Adv. Polym. Sci.* **1999**, 107−147.

(3) Yurekli, K.; Krishnamoorti, R.; Tse, M. F.; McElrath, K. O.; Tsou, A. H.; Wang, H.-C. *J. Polym. Sci., Part B: Polym. Phys. Ed.* **2001**, *39*, 256−275.

(4) Theng, B. K. G. *The Chemistry of Clay-Organic Reactions*; John Wiley and Sons: New York, 1974. Solomon, D. H.; Hawthorne, D. G. *Chemistry of Pigments and Fillers*; Krieger: Malabar, FL, 1991.

(5) Theng, B. K. G. *Formation and Properties of Clay Polymer Complexes*; Elsevier: New York, 1979.

(6) Usuki, A.; Kojima, Y.; Kawasumi, M.; Okada, A.; Fukushima, Y.; Kurauchi, T.; Kamigaito, O. *J. Mater. Res.* **1993**, *8*, 1179. Kojima, Y.; Usuki, A.; Kawasumi, M.; Okada, A.; Fukushima, Y.; Kurauchi, T.; Kamigaito, O. *J. Mater. Res.* **1993**, 1185. Yano, K.; Usuki, A.; Okada, A.; Kurauchi, T.; Kamigaito, O. *J. Polym. Sci., Part A: Polym. Chem.* **1993**, *31*, 2493. Manias, E.; Touny, A.; Wu, L.; Strawhecker, K.; Lu, B.; Chung, T. C. *Chem. Mater.* **2001**, *13*, 3516−3523.

(7) Mitchell, C. A.; Krishnamoorti, R. *J. Polym. Sci., Part B: Polym. Phys. Ed.* **2002**, *40*, 1434−1443.

(8) Krishnamoorti, R.; Silva, A. S. In *Polymer-Clay Nanocomposites*; Pinnavaia, T. J., Beall, G. W., Eds.; John Wiley & Sons: New York, 2000; pp 315−343.

(9) Krishnamoorti, R.; Silva, A. S.; Mitchell, C. A. *J. Chem. Phys.* **2001**, *108*, 7175.

(10) Vaia, R. A.; Giannelis, E. P. *Macromolecules* **1997**, *30*, 7990−7999. Vaia, R. A.; Jandt, K. D.; Kramer, E. J.; Giannelis, E. P. *Macromolecules* **1995**, *28*, 8080−8085. Wong, S.; Vasudevan, S.; Vaia, R. A.; Giannelis, E. P.; Zax, D. *J. Am. Chem. Soc.* **1995**, *117*, 7568.

(11) Krishnamoorti, R.; Yurekli, K. *Curr. Opin. Colloid Interface Sci.* **2001**, *6*, 464−470.

(12) Ren, J.; Silva, A. S.; Krishnamoorti, R. *Macromolecules* **2000**, *33*, 3739−3746.

(13) Mitchell, C. A.; Krishnamoorti, R. In *Polymer Nanocomposites*; Krishnamoorti, R., Vaia, R. A., Eds.; American Chemical Society: Washington, DC, 2001; Vol. 804, pp 159−175.

(14) Choi, H. J.; Kim, S. G.; Hyun, Y. H.; Jhon, M. S. *Macromol. Rapid Commun.* **2001**, *22*, 320−325. Fornes, T. D.; Yoon, P. J.; Keskkula, H.; Paul, D. R. *Polymer* **2001**, *42*, 9929−9940. Solomon, M. J.; Almusallam, A. S.; Seefeldt, K. F.; Somwangthanaroj, A.; Varadan, P. *Macromolecules* **2001**, *34*, 1864−1872. Galgali, G.; Ramesh, C.; Lele, A. *Macromolecules* **2001**, *34*, 852−858. Hoffmann, B.; Dietrich, C.; Thomann, R.; Friedrich, C.; Mulhaupt, R. *Macromol. Rapid Commun.* **2000**, *21*, 57−61. Okamoto, M.; Nam, P. H.; Maiti, P.; Kotaka, T.; Hasegawa, N.; Usuki, A. *Nano Lett.* **2001**, *1*, 295−298. Schmidt, G.; Nakatani, A. I.; Butler, P. D.; Karim, A.; Han, C. C. *Macromolecules* **2000**, *33*, 7219−7222.

(15) Krishnamoorti, R.; Giannelis, E. P. *Langmuir* **2001**, *17*, 1448−1452.

(16) Krishnamoorti, R.; Ren, J.; Silva, A. *J. Chem. Phys.* **2001**, *114*, 4968−4973.

(17) Krishnamoorti, R.; Vaia, R. A.; Giannelis, E. P. *Chem. Mater.* **1996**, *8*, 1728.

(18) Krishnamoorti, R.; Giannelis, E. P. *Macromolecules* **1997**, *30*, 4097.

(19) Sollich, P.; Lequeux, F.; Hebraud, P.; Cates, M. E. *Phys. Rev. Lett.* **1997**, *78*, 2020−2023. Sollich, P. *Phys. Rev. E* **1998**, *58*, 738−759.

(20) Fielding, S. M.; Sollich, P.; Cates, M. E. *J. Rheol.* **2000**, *44*, 323−369. Bonn, D.; Tanase, S.; Abou, B.; Tanaka, H.; Meunier, J. *Phys. Rev. Lett.* **2002**, *89*, 015701. Cloitre, M.; Borrega, R.; Leibler, L. *Phys. Rev. Lett.* **2000**, *85*, 4819−4822.

(21) Holmqvist, P.; Castelletto, V.; Hamley, I. W.; Hermsdorf, N.; Almdal, K. *Polymer* **2001**, *42*, 7203−7208.

(22) Watanabe, H.; Sato, T.; Osaki, K. *Macromolecules* **1996**, *29*, 3890. Watanabe, H.; Yao, M.; Sato, T.; Osaki, K. *Macromolecules* **1997**, *30*, 5905. Watanabe, H.; Yao, M.; Osaki, K.; Shikata, T.; Niwa, H.; Morishima, Y. *Rheol. Acta* **1997**, *36*, 424. Watanabe, H.; Yao, M.; Osaki, K.; Shikata, T.; Niwa, H.; Morishima, Y.; Balsara, N. P.; Wang, H. *Rheol. Acta* **1998**, *37*, 1. Yurekli, K.; Krishnamoorti, R. *Macromolecules* **2002**, *35*, 4075−4083.

(23) Silva, A. S.; Mitchell, C. A.; Tse, M. F.; Wang, H.-C.; Krishnamoorti, R. *J. Chem. Phys.* **2001**, *108*, 7166.

(24) Osaki, K. *Rheol. Acta* **1993**, *32*, 429−437.

(25) Vrentas, C. M.; Graessley, W. W. *J. Rheol.* **1982**, *26*, 359−371.

(26) Foster, M. D.; Sikka, M.; Singh, N.; Bates, F. S. *J. Chem. Phys.* **1992**, *96*, 8605−8615. Hajduk, D. A.; Tepe, T.; Takenouchi, H.; Tirrell, M.; Bates, F. S.; Almdal, K.; Mortensen, K. *J. Chem. Phys.* **1998**, *108*, 326−333. Fredrickson, G. H.; Helfand, E. *J. Chem. Phys.* **1988**, *89*, 5890−5897. Bates, F. S.; Koppi, K. A.; Tirrell, M.; Almdal, K.; Mortensen, K. *Macromolecules* **1994**, *27*, 5934−5936. Onuki, A. *J. Phys.: Condens. Matter* **1997**, *9*, 6119−6157.

(27) Foster, S.; Khandpur, A. K.; Zhao, J.; Bates, F. S.; Hamley, I. W.; Ryan, A. J.; Bras, W. *Macromolecules* **1994**, *27*, 6922−6934.

(28) Lin, C. C.; Jonnalagadda, S. V.; Kesani, P. K.; Dai, H. J.; Balsara, N. P. *Macromolecules* **1994**, *27*, 7769−7780.

(29) Han, C. D.; Kim, S. S. *J. Rheol.* **1994**, *38*, 31−40.

(30) Papanastasiou, A. C.; Scriven, L. E.; Maccoko, C. W. *J. Rheol.* **1983**, *27*, 387.

(31) Mackley, M. R.; Marshall, R. T. J.; Smeulders, J.; Zhao, F. D. *Chem. Eng. Sci.* **1994**, *49*, 2551−2565.

(32) Sanaa, F.; Gharbia, M.; Gharbi, A.; Nguyen, H. T. *Surf. Sci.* **2002**, 93−100. Mewis, J.; Moldenaers, P. *Curr. Opin. Colloid Interface Sci.* **1996**, *1*, 466−471. Iza, M.; Bousmina, M. *J. Rheol.* **2000**, *44*, 1363−1384.

(33) Larson, R. *The Structure and Rheology of Complex Fluids*; Oxford University Press: New York, 1999.

(34) Manias, E.; Bitsanis, I.; Hadziioannou, G.; ten Brinke, G. *Europhys. Lett.* **1996**, *33*, 371.

(35) In previous measurements of alignment starting with large-amplitude oscillatory shear (i.e., 100% or higher), the torque signal was found to possess in the first few cycles a third-order harmonic signal that was less than 5% of the primary harmonic and reduced in the later cycles. In the present experiments the strain amplitude is gradually increased, and we anticipate that even at the highest strain amplitudes

accessed, the primary harmonic would dominate the viscoelastic response.
(36) Malkin, A. Y. *Adv. Polym. Sci.* **1990**, *96*, 69.
(37) Hammouda, B.; Mang, J.; Kumar, S. *Phys. Rev. E* **1995**, *51*, 6282−6285. Burghardt, W. R. *Macromol. Chem. Phys.* **1998**, *199*, 471−488.
(38) Gu, D.-F.; Jamieson, A. M.; Wang, S.-Q. *J. Rheol.* **1993**, *37*, 985−1001. Gu, D.-F.; Jamieson, A. M. *J. Rheol.* **1994**, *38*, 555−571. Barbosa, S. E.; Bibbq, M. A. *J. Polym. Sci., Part B: Polym. Phys.* **2000**, *38*, 1788−1799.
(39) Enikolopyan, N. S.; Fridman, M. L.; Stalnova, I. O.; Popov, V. L. *Adv. Polym. Sci.* **1990**, *96*, 1−67.
(40) Dealy, J. M. *Rheometers for Molten Plastics*; Van Nostrand Reinhold Co.: New York, 1982.
(41) Laun, H. M. *Colloid Polym. Sci.* **1984**, *262*, 257−269.
(42) Bernstein, B.; Kearsley, E. A.; Zapas, L. J. *Trans. Soc. Rheol.* **1963**, *7*, 391−410.
(43) Larson, R. G. *Constitutive Equations for Polymer Melts and Solutions*; Butterworth: Boston, 1988. Lodge, A. S. *Elastic Liquids*; Academic Press: New York, 1964. Laun, H. M. *J. Rheol.* **1986**, *30*, 459−501.

MA020412N